Dynamic quantitative microscopy and nanoscopy of red blood cells in sickle cell disease

Natan T. Shaked*[a], Lisa L. Satterwhite[b], Marilyn J. Telen[c], George A. Truskey[b], and Adam Wax[b]

[a] Department of Biomedical Engineering and the Nano Center, Faculty of Engineering, Tel Aviv University, Tel Aviv 69978, Israel.
[b] Department of Biomedical Engineering, Fitzpatrick Institute for Photonics, Duke University Durham, North Carolina 27708, USA.
[c] Division of Hematology, Department of Medicine, Duke University Medical Center, Durham, North Carolina 27708, USA.

ABSTRACT

We have applied wide-field digital interferometric techniques to quantitatively image sickle red blood cells (RBCs) [1] in a noncontact label-free manner, and measure the nanometer-scale fluctuations in their thickness as an indication of their stiffness. The technique can simultaneously measure the fluctuations for multiple spatial points on the RBC and thus yields a map describing the stiffness of each RBC in the field of view. Using this map, the local rigidity regions of the RBC are evaluated quantitatively. Since wide-field digital interferometry is a quantitative holographic imaging technique rather than one-point measurement, it can be used to simultaneously evaluate cell transverse morphology plus thickness in addition to its stiffness profile. Using this technique, we examine the morphology and dynamics of RBCs from individuals who suffer from sickle cell disease, and find that the sickle RBCs are significantly stiffer than healthy RBCs. Furthermore, we show that the technique is sensitive enough to distinguish various classes of sickle RBCs, including sickle RBCs with visibly-normal morphology, compared to the stiffer crescent-shaped sickle RBCs.

Keywords: Interferometric phase microscopy, holographic microscopy, red blood cells, sickle cell disease.

1. INTRODUCTION

Sickle cell disease (SCD) is a genetic blood disorder that is common in people from tropical regions where malaria has been widespread, such as Sub-Saharan Africa. SCD is caused by a single-point mutation in the hemoglobin gene, termed hemoglobin S, which leads to polymerization of deoxygenated hemoglobin. Red blood cells (RBCs) of a person with SCD tend to be fragile and less-flexible than normal RBCs. When deoxygenated, sickle RBCs assume a distorted and often crescent shape. RBC abnormalities include deformation, dehydration, and increased adhesivity, which cause multisystem dysfunctions associated with the disease [2], including vaso-occlusive crisis due to vascular obstruction resulting in ischemia and severe pain, as well as splenic sequestration crisis, aplastic crisis, and haemolytic crisis. Average life expectancy of individuals with SCD is 42-48 years. Changes in mechanical properties of sickle RBCs are attributed both to cell wide polymerization of hemoglobin into complex and dynamic fiber systems and to increased association of hemoglobin S with the membrane proteins [3], among other processes. Improved understanding of the relationship between the physical properties of sickle RBCs and the resulting dynamic behaviors is needed urgently to improve detection, monitoring and potential treatments for SCD [4].

Sickle RBCs have been measured by various invasive, contact-based, or force application methods such as micropipette aspiration, cell poking, optical stretching, magnetic twisting cytometry, atomic force microscopy, and optical tweezers [5-8].

WFDI is a non-contact holographic technique that is able to record the entire complex wavefront (amplitude and phase) of the light which has interacted with the sample by using a low-power partially-coherent laser light, where no exogenous labeling or special sample preparations are involved. Using the recorded interference pattern, one can obtain the quantitative phase profile of the sample representing the optical path delay map for each spatial point in the sample image. This map is dependent in both the integral refractive index of the sample and its thickness. We have previously

shown that WFDI is applicable for studying cancer cells, chondrocytes, neurons, and cardiomyocytes [9-14]. Mature (enucleated) red blood cells are an attractive goal for WFDI since they can be assumed to have homogenous refractive index structure and thus RBC thickness profiles can be obtained directly from their quantitative phase profile. WFDI has been used to measure various morphological and dynamic parameters of RBCs [15-19], including during malaria [20].

We have applied [1] WFDI techniques to quantitatively image sickle RBCs and to measure the nanometer-scale fluctuations in their thickness as an indication of their stiffness. The technique is capable of simultaneously measuring the fluctuations for multiple spatial points on the RBC and thus can yield a map describing the stiffness of each RBC in the field of view. Using this map, the local rigidity regions of each cell can be evaluated quantitatively. Furthermore, since the technique is basically a quantitative imaging technique rather than one-point measurement, we can use it to simultaneously evaluate cell transverse morphology plus thickness in addition to its stiffness profile. Thus, the technique yields various physical properties for live RBCs in a noninvasive, label-free manner, providing a sensitive tool for diagnosis and research.

2. MEASURING RBCs USING WFDI

Single-exposure WFDI setup can be based, for example, on the Mach-Zehnder interferometer and an off-axis holographic geometry [21]. In this optical setup, light from a coherent source (HeNe laser, for example) is first spatially filtered using a pair of spherical lenses and a confocally-positioned pinhole, and then split into reference and object beams by beam splitter. The object beam is transmitted through the sample and magnified by a microscope objective. The reference beam is transmitted through a compensating microscope objective (typically similar to the object-beam objective) and then combined with the object beam at an angle. The combined beams are projected onto a digital camera by a tube lens, which is postioned in a 4f configuration with each of the microscope objectives, meaning that the distance between each of the microscope objectives and the tube lens is equal to the summation of their focal lengths. This configuration allows projection of the amplitude and phase distribution of the sample onto the camera. The combination of the sample and reference beams creates a high spatial frequency off-axis hologram of the sample on the digital camera. The digital off-axis hologram acquired by the camera is the summation of the object and reference waves, and can be mathematically expressed as follows:

$$H(x,y) = |E_S + E_r|^2 = |E_S|^2 + |E_r|^2 + |E_S||E_r^*|\cos[(\phi(x,y)+qx], \tag{1}$$

where E_S and E_r are respectively the sample and reference field distributions, $\phi(x,y)$ is the spatially-varying phase associated with the sample, q is the fringe frequency due to the angular shift between the sample and reference fields, x is the direction of the angular shift (assuming linear horizontal fringes in the off-axis hologram).

The common digital processing method applied to the off-axis hologram starts with a digital two-dimensional Fourier transform. The resulting spatial-frequency contents includes reference-field and sample-field autocorrelations (as a result of transforming the first two elements of Eq. (1)) that are located around the origin of the spatial spectrum, and two mathematically conjugated cross-correlation terms (as a result of transforming the cosine term in Eq. (1)), each located at a different side of the spatial spectrum. The exact locations of the cross-correlation terms are dependent on the angle between the object and reference beams. Looking at the spectrum profile, it is easy to isolate only one of the cross-correlation terms, center it, and perform a digital two-dimensional inverse Fourier transform on the result, yielding $|E_S||E_r^*|\exp[j(\phi(x,y)]$. Assuming a weak amplitude modulation due to the transparancy of biological cells in culture, the phase argument of the result $\phi(x,y)$ is the phase profile of the sample.

This WFDI setup is also reported in detail in our previous publication [9]. In this previous paper, we have used the system for quantitative microscopy of cardiomyocytes, in which thickness and refractive index cannot be easily decoupled. As shown next, this is not the case for RBCs, in which thickness and stiffness measurements can be easily performed by WFDI. In the optical setup, a coherent laser light (17mW HeNe) is spatially filtered and split to reference and object beams. The object beam is transmitted through the sample and magnified by a microscope objective (40×, 0.66 numerical aperture). The reference beam passes through a similar compensating microscope objective and combined with the object beam at a small angle. A tube lens projects the combined fields on a digital camera (640×480, 7.4μm×7.4μm pixels, 120 full frames per second), where an off-axis interferogram of the sample is created. Using a single interferogram, the fully quantitative phase profile of the sample is obtained by an improved spatial filtering process that is performed in the image domain [13], followed by a quality-guided phase-unwrapping algorithm.

The spatially varying phase measured by WFDI is defined as follows:

$$\phi(x,y) = \frac{2\pi}{\lambda}\left[\bar{n}_c(x,y)h_c(x,y) + n_m(h_m - h_c(x,y))\right]$$

$$= \frac{2\pi}{\lambda}\left[(\bar{n}_c(x,y) - n_m)h_c(x,y) + n_m h_m\right], \tag{2}$$

where λ is the illumination wavelength, $n_c(x,y)$ is the spatially varying integral refractive index, $n_m = 1.340$ is the medium refractive index, $h_c(x,y)$ is the spatially varying thickness profile of the cell, and h_m is the thickness of the cell medium.

Various morphological parameters that are useful for cell biologists, including cell volume and cell force distribution, are based on the thickness profile of the cell rather than on the phase profile. Many methods have been developed to decouple thickness from refractive index difference using the cell phase profile [21]. However, for mature RBCs, a constant refractive index can be assumed for the entire cell contents (e.g. $\bar{n}_c \cong 1.395$) [15-17]. Therefore, the thickness profile can be directly obtained from the phase profile. Since WFDI is able to record the quantitative thickness profile of the RBCs, and since only a single frame of acquisition (one interferogram) is needed for obtaining this profile, it is possible to measure rapid thickness changes indicating on the RBC membrane fluctuations. These fluctuations can reveal various medical conditions and blood diseases [15-20].

3. SICKLE RBC EXPERIMENTS

We used WFDI to measure membrane fluctuations of sickle and healthy RBCs [1]. For the experiments, blood samples were obtained from the Comprehensive Sickle Cell Programs in Duke University and in the University of North Carolina at Chapel Hill and adhered to approved Institutional Review Board (IRB) protocols. The samples were obtained from two donors with SCD and from a healthy donor. Whole blood was collected in a 4.0 ml K$_2$EDTA Vacutainer tube (BD367861) or by needle stick and was stored at 4°C. A 50 μl aliquot was washed twice in 1.0 ml Hanks Balanced Salt Solution (HBSS) without calcium, magnesium or phenol red (Invitrogen/Gibco 14175), and resuspended in a 2:1 mixture of endothelial basal media 2 (EBM-2) that contained growth supplements, and 10% fetal bovine serum (Lonza) that contained 10% fetal bovine serum and HBSS. Glass coverslips (22mm×50mm) were treated with 100 μl 1.0 mg/ml poly-D-lysine hydrobromide (SigmaAldrich P7280) in dH$_2$O for 1 hour at 37°C, residual solution aspirated, and 50 μl of the blood cell suspension allowed to attach for 30 min at 37°C. Attached cells were washed briefly in EBM:HBSS before imaging at 22°C.

Figure 1(a) presents the quantitative phase profile of the RBCs from a healthy person, demonstrating the characteristic round-biconcave shape which, by allowing an increased surface:volume ratio, facilitates diffusion into and out of the cell and helps deliver oxygen to body tissues, as well as increases cell deformability. The colorbar in the right side of Fig. 1 can be used to interpret the quantitative maps in terms of cell thickness. This interpretation is correct if a constant refractive index can be assumed for the entire cell thickness, which, as mentioned before, is a valid assumption for healthy RBCs. For sickle RBCs, this assumption is mostly correct, except perhaps in areas where polymerized hemoglobin is present, typically in thin (~20 nm diameter) rod-like fibers spanning the RBCs [3]. In any case, the optical path delay profile can also be used directly to obtain stiffness information, even without calculating the thickness profile.

Figure 1(b) presents the quantitative phase profile of the RBCs of a person with SCD. As seen in this figure, only a fraction of the sickle RBCs have lost their round-biconcave shape and becomes crescent shaped.

In contrast to conventional microscopy, WFDI allows quantitative dynamic analysis of the thickness fluctuations of the RBCs for each spatial point on the cell and for each of the cells in the field of view. We have acquired phase profiles of 24 RBCs obtained from two different persons with SCD and 12 RBCs obtained from a healthy person. For each RBC, phase profiles were collected at a frame rate of 120 frames per second during 10 seconds and converted into thickness profiles. For each cell, we have calculated the standard deviation of the thickness fluctuations σ_h, which is inversely proportional to the stiffness map of the RBC [15,16]. Averaging σ_h over the entire RBC area, marked as $\langle \sigma_h \rangle$, gives an indication of the cell flexibility, since less rigid RBCs are expected fluctuate more than stiffer RBCs.
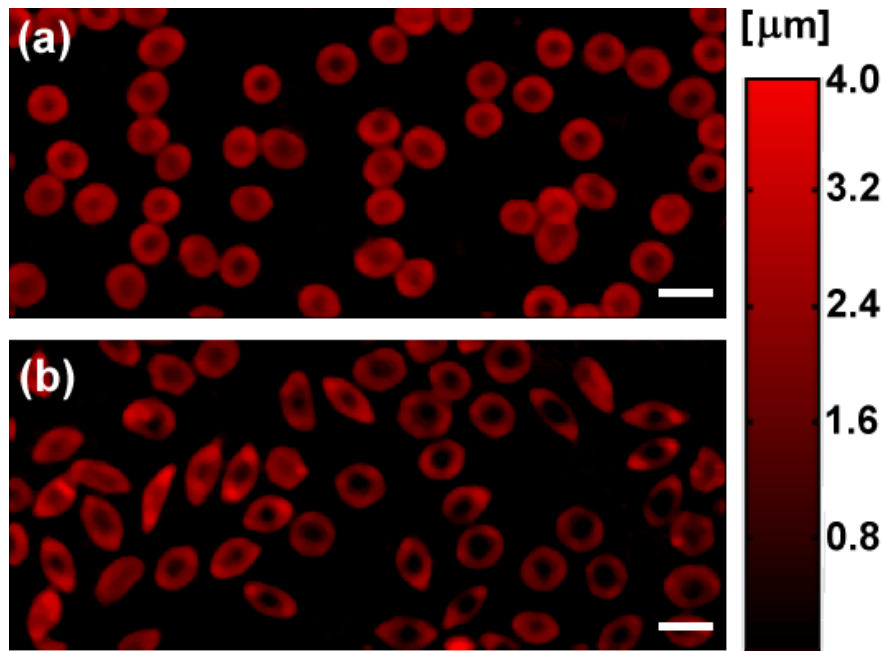
Figure 1. WFDI quantitative phase imaging of: (a) healthy RBCs, (b) Sickle RBCs, demonstrating the different RBC morphology that characterizes SCD. Quantitative thickness profile can be obtained for each of the cells in the field of view. Scale bar represents 10 µm. Color bar represents thickness in µm [1].

Figure 2 presents the quantitative phase profile and the associated thickness scalebar for one of the analyzed RBCs obtained from the healthy person (also see Video 1 in [1]). This specific cell yielded a standard deviation of the thickness fluctuations averaged over the cell area of $\langle\sigma_h\rangle$ = 64.12 nm. For comparison, Fig. 3 presents the quantitative phase profiles and the associated thickness scalebar of two RBCs obtained from a person with SCD (also see Video 2 in [1]). As can be seen in this figure, the right cell has a regular round morphology, whereas the left cell has a crescent morphology. For these sickle RBCs, the standard deviation of the thickness fluctuations averaged over each of the cell areas is $\langle\sigma_h\rangle$ = 28.73 nm for the round-morphology RBC and $\langle\sigma_h\rangle$ = 13.54 nm for the crescent-morphology RBC. Thus, even though the sickle RBC on the right has a visibly normal morphology, it is found to be more than twice as stiff as the healthy RBC. The cells were well adhered to the coverslip by positioning them on poly-D-lysine substrate. Thus, only thickness fluctuations were measured by the WFDI setup, rather than fluctuations due to movement of the cells.

Figure 4 presents $\langle\sigma_h\rangle$ values obtained for RBCs of three groups: 12 round-morphology RBCs from a healthy person, 12 round-morphology RBCs from two persons with SCD, and 12 crescent-morphology RBCs from two persons with SCD.

Each of the two groups of 12 sickle RBCs was composed of 5-7 RBCs from the first person with SCD and 5-7 RBCs from the second person with SCD, where no significant difference was seen between the $\langle\sigma_h\rangle$ values of the RBCs from the two individuals with SCD. The healthy RBCs yielded $\langle\sigma_h\rangle = 51.07 \pm 12.02$ nm (which compares favorably with the values obtained for healthy RBCs by Park et al. [16]), the round-morphology RBCs from SCD individuals yielded $\langle\sigma_h\rangle = 21.76 \pm 7.64$ nm, and the crescent-morphology RBCs from SCD individuals yielded $\langle\sigma_h\rangle = 13.82 \pm 3.92$ nm. These results demonstrate that the healthy RBCs are 2-3 times less stiff than the round-morphology sickle RBCs, and the latter are approximately half as stiff as the sickle crescent-morphology RBCs. Greater statistical difference, indicated by the lower p-values ($p < 0.001$), is obtained between the group of healthy RBCs and each group of the sickle RBCs than between the two groups of sickle RBCs ($p < 0.05$). The high statistical significance of the difference between the round-morphology RBCs from SCD individuals and the healthy RBCs demonstrates that although the sickle RBC shape might visibly appear to be the same as healthy RBCs, analyzing their thickness fluctuations by WFDI gives a clear indication that they are sickle RBCs.
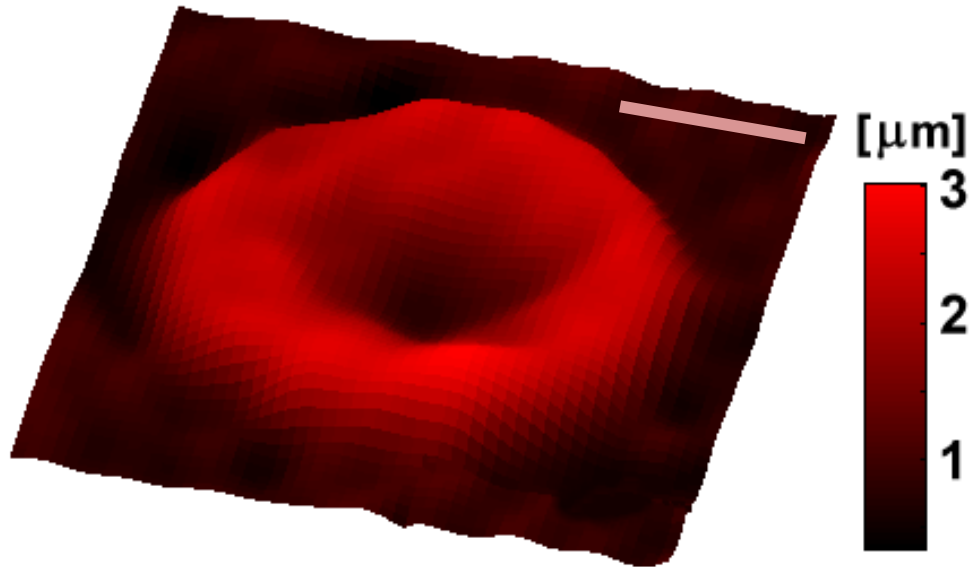
Figure 2. WFDI quantitative phase profile of a healthy RBC. Scale bar represents 3 μm. Color bar represents thickness in μm. See also Video 1 in [1].
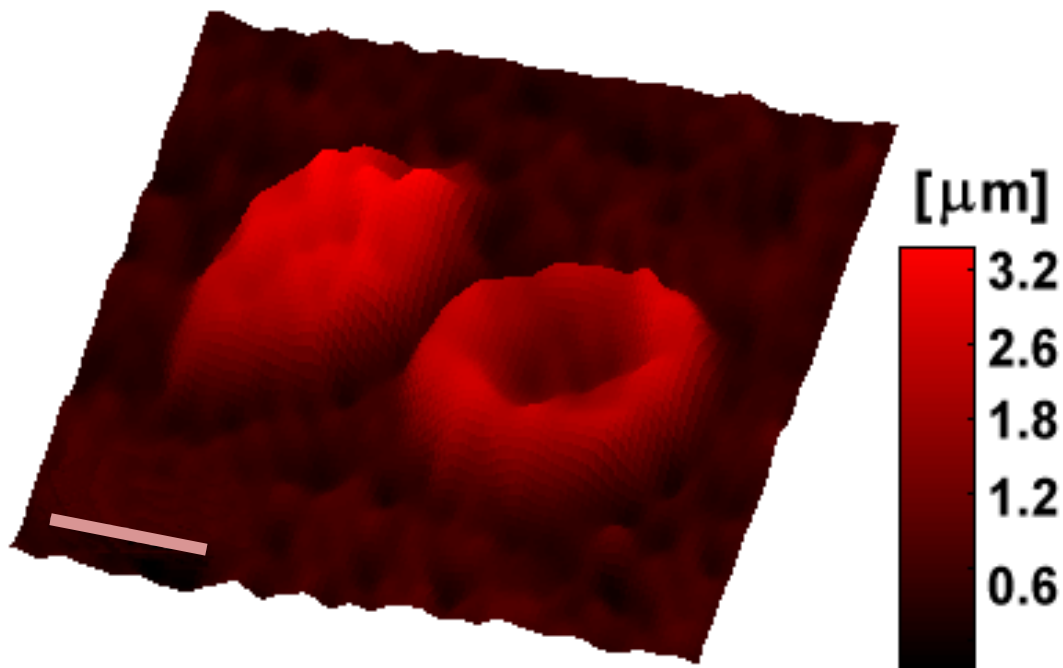

Figure 3. WFDI quantitative phase profile of two RBCs obtained from a person with SCD, the right one with round morphology (visibly healthy) and the left one with crescent morphology. The crescent-morphology cell fluctuates less than the round-morphology cell. Scale bar represents 5 μm. Color bar represents thickness in μm. See also Video 2 in [1].
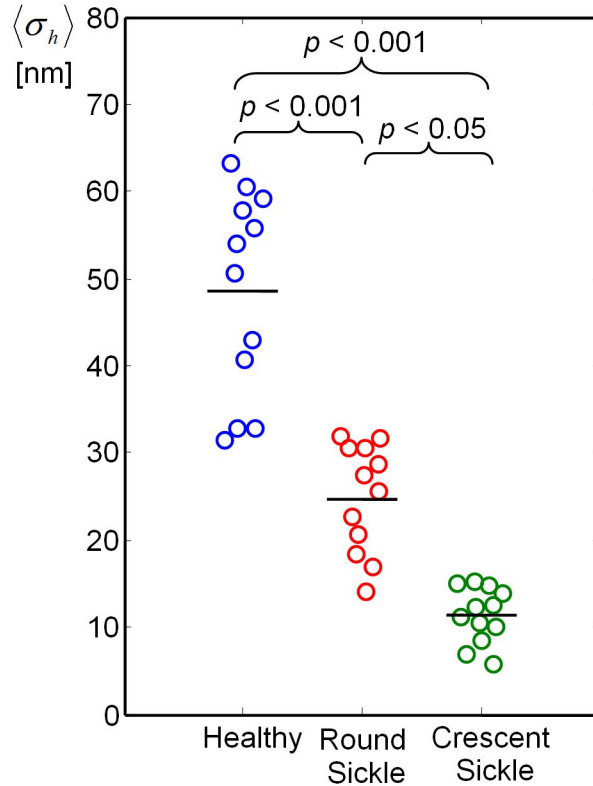
Figure 4. Averaged standard deviation of the thickness fluctuations $\langle \sigma_h \rangle$ of RBCs on poly-D-lysine substrate obtained from the WFDI dynamic phase profiles of RBCs of three groups: round (typical) morphology RBCs from a healthy person, round (visibly-healthy) morphology RBCs from persons with SCD, and crescent-morphology RBCs from persons with SCD. Each circle represents a different RBC, and the horizontal line at each group represents the average value of all cells in the group. *p*-values were calculated by the two-sided Wilcoxon rank-sum test [1].

4. CONCLUSIONS

We have demonstrated that WFDI is able to obtain dynamic quantitative phase profiles of sickle RBCs in a noncontact, noninvasive manner [1]. Based on these profiles, we have calculated the nanometer-scale thickness fluctuations of the RBCs and obtained a metric of RBC stiffness. Sickle RBCs were found to be significantly stiffer than healthy RBCs. Furthermore, we have demonstrated that it is possible to differentiate between sickle RBC morphologies taken from the same subjects by analyzing their thickness fluctuations, where crescent-morphology RBCs are more rigid (fluctuate less) than round-morphology RBCs. We anticipate that this technique will find uses for diagnosis and monitoring of SCD, as well as usefulness as a research tool, since therapeutic agents that decrease sickling can be expected to improve the abnormal cell rigidity described here. In addition to helping identify and prove the effectiveness of new SCD therapeutic approaches, this technique might be useful in differentiating SCD from sickle cell trait, a condition in which there is one gene for the formation of hemoglobin S and one for the formation of normal hemoglobin. Usually, people with sickle cell trait live relatively healthy lives but if their partner has sickle cell trait as well, there is 25% chance that their child will have sickle cell disease. Sickle-trait cells generally do not form sickled cells, and the simplest test for hemoglobin S cannot distinguish between SCD and sickle cell trait.

REFERENCES

[1]   Shaked, N. T., Satterwhite, L. L., Truskey, G. A., Telen, M. J., and Wax, A., "Quantitative microscopy and nanoscopy of sickle red blood cells performed by wide field digital interferometry," *Journal of Biomedical Optics Letters* 16, 030506 (2011).

[2]   Ballas, S. K., Lieff, S., Benjamin, L. J., Dampier, C. D., Heeney, M. M., Hoppe, C., Johnson, C. S., Rogers, Z. R., Smith-Whitley, K., Wang, W. C., and Telen, M. J., "Definitions of the phenotypic manifestations of sickle cell disease," Am. J. Hematol. 85, 6-13 (2010)

[3]   Statius van Eps, L. W., "Sickle cell disease," in [Atlas of Diseases of the Kidney], Schrier, R.W. (Ed.), Vol. 4, Current Medicine, Inc., Philadelphia, PA (1999).

[4]   Suresh, S. "Mechanical response of human red blood cells in health and disease: some structure–property-–function relationships," Journal of Materials Research 21, 1871-1877 (2006).

[5]   Barabino, G. A., Platt, M. O., and Kaul, D. K., "Sickle Cell Biomechanics," Annual Review of Biomedical Engineering 12, 345-367 (2010).

[6]   Ballas, S. K. and Mohandas, N., "Sickle Red Cell Microrheology and Sickle Blood Rheology," Microcirculation, 11, 209-225 (2004).

[7]   Brandao, M. M., Fontes, A., Barjas-Castro, M. L., Barbosa, L. C., Costa, F. F., Cesar, C. L., and Sead, S. T. O., "Optical tweezers for measuring red blood cell elasticity: Application to the study of drug response in sickle cell disease," Eur. J. Haematol. 70, 207-211 (2003).

[8]   Maciaszek, J. L. and Lykotrafitis, G., "Sickle cell trait human erythrocytes are significantly stiffer than normal," Journal of Biomechanics 44, 657-661 (2011).

[9]   Shaked, N. T., Satterwhite, L. L., Bursac, N., and Wax, A., "Whole-cell-analysis of live cardiomyocytes using wide-field interferometric phase microscopy," Biomedical Optics Express 1, 706-719 (2010).

[10]   Shaked, N. T., Zhu, Y., Badie, N., Bursac, N., and Wax, A., "Reflective interferometric chamber for quantitative phase imaging of biological sample dynamics," Journal of Biomedical Optics Letters 15, 030503 (2010).

[11]   Shaked, N. T., Newpher, T. M., Ehlers, M. D., and Wax, A., "Parallel on-axis holographic phase microscopy of biological cells and unicellular microorganism dynamics," Applied Optics 49, 2872-2878 (2010).

[12]   Shaked, N. T., Finan, J. D., Guilak, F., and Wax, A., "Quantitative phase microscopy of articular chondrocyte dynamics by wide-field digital interferometry," Journal of Biomedical Optics Letters 15, 010505 (2010).

[13]   Shaked, N. T., Zhu, Y., Rinehart, M. T., and Wax, A., "Two-step-only phase-shifting interferometry with optimized detector bandwidth for microscopy of live cells," Optics Express 17, 15585-15591 (2009).

[14]   Shaked, N. T., Rinehart, M. T., and Wax, A., "Dual-interference-channel quantitative-phase microscopy of live cell dynamics," Optics Letters 34, 767-769 (2009).

[15]   Popescu, G., Park, Y. K., Choi, W., Dasari, R. R., Feld, M. S., and Badizadegan, K., "Imaging red blood cell dynamics by quantitative phase microscopy," Blood Cells, Molecules, and Diseases 41, 10-16 (2008).

[16]   Park, Y. K., Best, C. A., Auth, T., Gov, N. S., Safran, S. A., Popescu, G., and Suresh, S., "Metabolic remodeling of the human red blood cell membrane," Proc. Natl. Acad. Sci. USA 107, 1289-1294 (2010).

[17]   Rappaz, B., Barbul, A., Emery, Y., Korenstein, R., Depeursinge, C., Magistretti, P. J., and Marquet, P., "Comparative study of human erythrocytes by digital holographic microscopy, confocal microscopy, and impedance volume analyzer," Cytometry 73A, 895-903 (2008).

[18]   Brazhe, R., Brazhe, N. A., Maksimov, G. V., Ignatyev, P. S., Rubin, A. B., Mosekilde, E., and Sosnovtseva, O. V., "Phase-modulation laser interference microscopy: an advance in cell imaging and dynamics study," Journal of Biomedical Optics 13, 034004 (2008).

[19]   Yusipovich, A. I., Yu. Parshina, E., Yu. Brysgalova, N., Brazhe, A. R., Brazhe, N. A., Lomakin, A. G., Levin, G. G., and Maksimov, G. V., "Laser interference microscopy in erythrocyte study," Journal of Applied Physics 105, 102037 (2009).

[20]   Park, Y. K., Diez-Silva, M., Popescu, G., Lykorafitis, G., Choi, W., Feld, M. S., and Suresh, S., "Refractive index maps and membrane dynamics of human red blood cells parasitized by plasmodium falciparum," Proc. Natl. Acad. Sci. USA 105, 13730-13735 (2008).

[21]   Shaked, N. T. and Wax, A., "Quantitative Analysis of Biological Cells Using Digital Holographic Microscopy," In [Holography, Research and Technologies], Joesph Rosen (Ed.), Intech (2011).